Environmental Science & Technology

pubs.acs.org/est

Article

Preparation and Synergy of Supported Ru^0 and Pd^0 for Rapid Chlorate Reduction at pH 7

Jinyu Gao, Shaohua Xie, Fudong Liu, and Jinyong Liu*

Cite This: *Environ. Sci. Technol.* 2023, 57, 3962−3970

Read Online

ACCESS | Metrics & More | Article Recommendations | Supporting Information

ABSTRACT: Chlorate (ClO_3^-) is a common water pollutant due to its gigantic scale of production, wide applications in agriculture and industry, and formation as a toxic byproduct in various water treatment processes. This work reports on the facile preparation, mechanistic elucidation, and kinetic evaluation of a bimetallic catalyst for highly active ClO_3^- reduction into Cl^-. Under 1 atm H_2 and 20 °C, Pd^{II} and Ru^{III} were sequentially adsorbed and reduced on a powdered activated carbon support, affording Ru^0−Pd^0/C from scratch within only 20 min. The Pd^0 particles significantly accelerated the reductive immobilization of Ru^{III} as >55% dispersed Ru^0 outside Pd^0. At pH 7, Ru−Pd/C shows a substantially higher activity of ClO_3^- reduction (initial turnover frequency >13.9 min^{-1} on Ru^0; rate constant at 4050 L h^{-1} g_{metal}^{-1}) than reported catalysts (e.g., Rh/C, Ir/C, Mo−Pd/C) and the monometallic Ru/C. In particular, Ru−Pd/C accomplished the reduction of concentrated 100 mM ClO_3^- (turnover number > 11,970), whereas Ru/C was quickly deactivated. In the bimetallic synergy, Ru^0 rapidly reduces ClO_3^- while Pd^0 scavenges the Ru-passivating ClO_2^- and restores Ru^0. This work demonstrates a simple and effective design for heterogeneous catalysts tailored for emerging water treatment needs.

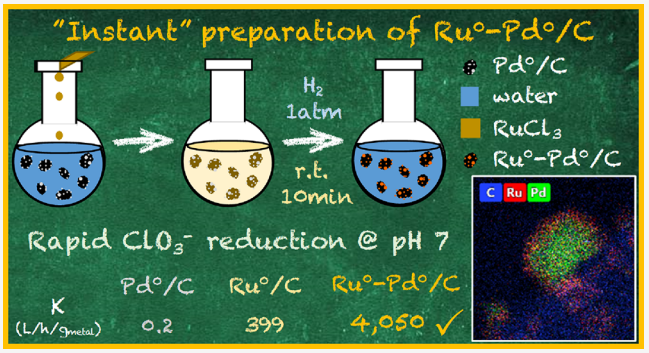

KEYWORDS: *ruthenium, palladium, in situ preparation, room temperature, chlorite, X-ray photoelectron spectroscopy (XPS), scanning transmission electron microscopy (STEM), dispersion*

INTRODUCTION

More than four million tons of sodium chlorate ($NaClO_3$) are manufactured annually worldwide for pulp bleaching, weed control, pyrotechnics, and so on.[1] Water disinfection using hypochlorite or chlorine dioxide[2] and various electrochemical processes (e.g., chloralkali,[3,4] water splitting,[5] seawater valorization,[6] and wastewater treatment[7]) also generate ClO_3^- as a byproduct.[8,9] Not surprisingly, ClO_3^- enters the water environment,[10−12] dairy supply chain,[13−16] and agricultural products.[17−19] When ingested, ClO_3^- can cause red blood cell rupture and thyroid gland malfunction.[20] The World Health Organization,[21] European Union,[22] and China[23] have set the limit of the ClO_3^- concentration in drinking water at 0.7 mg L^{-1}. The United States has set the health reference level at 0.21 mg L^{-1} and the minimum reporting level at 0.02 mg L^{-1}.[24,25] Hence, a highly efficient ClO_3^- reduction method will be of significant value for technological advances at the water−energy−food nexus.

Although the ClO_3^- challenge for water systems has been recently recognized,[2,20] research efforts for ClO_3^- reduction are limited. Platinum group metal (PGM)-catalyzed hydrogenation provides a clean degradation route:

$$ClO_3^- + 3\,H_2 \rightarrow Cl^- + 3\,H_2O$$

Besides, the ubiquitous use of PGM in automotive catalytic converters[26] and the negligible PGM leaching under the H_2 atmosphere[27,28] rationalize the application of PGM for water treatment.[28−30] However, most reported ClO_3^- reduction catalysts (e.g., Rh,[31] Ir,[32] Pd,[33] Mo−Pd[34]) exhibit maximum activity in acidic conditions. The proton-assisted mechanisms severely restrict the catalytic performance around neutral pH. If acidification is not feasible, a 10−80× dose of PGM catalyst is necessary to compensate for the activity loss and maintain the same reaction rate as at pH ≤ 4 (Table S1). Therefore, the priority of catalyst design is to integrate novel reaction mechanisms and pathways to achieve highly active ClO_3^- reduction at pH 7.

Previously, we observed the unique pH dependence of a commercial Ru/C for ClO_3^- reduction.[35] While carbon-supported Pd, Rh, Pt, and Ir lost activity by 90−98% from pH 3.0 to pH 7.2 (Table S1, entries 3−6 versus 10−13), Ru/C

Received: January 15, 2023
Revised: February 7, 2023
Accepted: February 7, 2023
Published: February 21, 2023

https://doi.org/10.1021/acs.est.3c00415
Environ. Sci. Technol. 2023, 57, 3962−3970

showed impaired function at pH 3.0 but outstanding activity at pH 7.2 (Table S1, entry 2 versus 9), indicating distinct working mechanisms of Ru from other PGMs. The following consideration is to develop a facile procedure to prepare the catalyst. Conventional catalysts developed for organic and gaseous reactions typically contained 5 wt % Ru in the porous support, and the preparation involved calcination at 400−500 °C and H_2 reduction at 300−450 °C.[36−39] For high-temperature catalysis, the thermal treatment removes undesirable species in the PGM precursor (e.g., Cl^- in $RuCl_3$), but it is unnecessary for water treatment because Cl^- is a ubiquitous water mineral, concentrated in brines and produced from ClO_3^- reduction. We have recently developed an all-in situ method to prepare Pd^0/C by adsorption of Pd^{II} in 5 min and reduction into Pd^0 with 1 atm H_2 at 20 °C in the next 5 min.[28] To meet the priority of both efficacy and simplicity for water technology development, we aimed to harness the unique catalytic activity of Ru and establish a convenient and reliable catalyst preparation method.

This work (i) achieves the unprecedented high activity of ClO_3^- reduction at pH 7 by harnessing the unique functions of Ru and Pd, (ii) develops a rapid and convenient preparation method for Ru^0−Pd^0/C catalyst with metal contents as low as 0.1 wt %, (iii) elucidates the structure and synergy of the two metals, and (iv) showcases the catalyst robustness under practical and challenging scenarios.

MATERIALS AND METHODS

Chemicals and Materials. $RuCl_3 \cdot xH_2O$ (99.98%), Na_2PdCl_4 (≥99.99%), $NaClO_3$ (≥99%), and $NaClO_2$ (technical grade, 80%) were used as received from Sigma-Aldrich. The activated carbon support (Norit GSX, steam activated and acid-washed, surface area 1300 $m^2\ g^{-1}$) was used as received from Alfa Aesar (#L11860). The alumina support was received as 1/8″ pellets from Alfa Aesar (#43855) and ground into powders before use.[28] A commercial 5 wt % Ru/C was purchased from Alfa Aesar (#44338) and dried at 70 °C before use. Except for the tap water, all aqueous solutions were prepared with Milli-Q water (resistivity >18.2 MΩ cm).

Catalyst Preparation. *All-In Situ Method for Pd/C and Ru−Pd/C.* A 50 mL flask was sequentially loaded with a magnetic stir bar, 5 mg of carbon support, 50 mL of DI water, and Na_2PdCl_4 stock solution. The mixture was sonicated for 1 min to disperse the carbon particles and stirred at 350 rpm for 4 min to allow the adsorption of Pd^{II}. The flask was then capped by a rubber stopper. A 16 G needle penetrating the stopper was connected to the H_2 gas supply (2−3 mL min^{-1}), and the needle tip was pushed under water. The other needle had the tip above the water as the gas outlet to the atmosphere. After 5 min of H_2 sparging at 20 °C, all adsorbed Pd^{II} was reduced to Pd^0.[28] After that, the Pd^0/C suspension was added with $RuCl_3$ stock solution and sparged with H_2 for another 10 min at 20 °C to reduce adsorbed Ru^{III} to Ru^0, yielding Ru^0−Pd^0/C.

All-In Situ Method for Ru/C and Pd−Ru/C. The preparation followed the same procedure as detailed above. However, the direct immobilization of Ru^{III} onto carbon took 1 h and the subsequent reduction by H_2 took 4 h to yield Ru^0/C. The immobilization of Pd^0 onto the resulted Ru^0/C still took 5 min for Pd^{II} adsorption and 5 min for the reduction by H_2, yielding Pd^0−Ru^0/C.

Conventional Method for Ru/C. The Ru^{III} precursor was impregnated into the same carbon support material by incipient wetness. The wet paste was first dried in an oven at 75 °C for 12 h and then reduced with 90/10 (v/v) N_2/H_2 at 450 °C for 6 h to yield Ru^0/C.[36,40]

Catalyst Characterization. The solid catalyst was collected from the water suspension by filtration under vacuum. The filter paper with the black paste was dried at 20 °C by the airflow in a fume hood. No inert gas protection was involved for catalyst handling or transportation. The Ru and Pd contents in the catalysts were measured by inductively coupled plasma−optical emission spectrometry (ICP-OES, PerkinElmer Optima 8300) after digestion at the Microanalysis Laboratory, University of Illinois at Urbana-Champaign. The oxidation state of Ru and Pd was characterized by X-ray photoelectron spectroscopy (XPS, Kratos AXIS Supra). The sp^2 C 1s peak (284.5 eV) of the carbon support was used for binding energy (BE) calibration. XPS spectra in the resolution of 0.1 eV were fitted using CasaXPS (version 2.3.19). Microscopic characterization was conducted using scanning transmission electron microscopy (STEM, FEI Titan Themis 300) equipped with an energy-dispersive X-ray spectrometer (EDS) system. The catalyst powder was resuspended and sonicated in distilled water to further reduce the size. The STEM images were acquired with a high-angle annular dark-field (HAADF) detector. Nano Measurer software package was used for the statistical analysis of average particle size in the STEM images. The specific surface areas of Ru and Pd were determined by CO pulse titration experiments on a Quantachrome Autosorb-iQ physisorption−chemisorption instrument. The calculation of metal dispersion used the surface Ru:CO and Pd:CO stoichiometry of 12:7[41] and 2:1,[42] respectively.

Chlorate and Chlorite Reduction. During the all-in situ catalyst preparation, the solution pH was significantly lowered from pH 6.5 (DI water with dissolved CO_2) because of the hydrolysis and reduction of $[Pd^{II}Cl_4]^{2-}$ and $Ru^{III}Cl_3$.[28,43] Therefore, the solution pH was adjusted by NaOH to pH 7.0 before adding ClO_3^- or ClO_2^-. The addition of 1 mM $NaClO_2$ stock solution increased the pH from 7.0 to 7.9 due to the hypochlorite impurity. However, as ClO_2^- is sensitive to acidic conditions,[44] we did not further adjust the pH back to 7.0 after the addition. The catalytic reduction of ClO_3^- and ClO_2^- started upon their spike into the catalyst suspension. The flow of 1 atm H_2 was maintained at 2−3 mL min^{-1}, and the flask reactor was placed on the benchtop (20 °C). Aliquots were collected through the H_2 outlet needle with a 3 mL plastic syringe and immediately filtered through a 0.22-μm cellulose acetate membrane.

The experiment with tap water (containing 0.4 mM NO_3^-) used a 50 mL double-neck flask. Both necks were capped with rubber stoppers. One stopper accommodated two needles as the H_2 inlet and outlet/sampling port, respectively. The other stopper accommodated a Fisherbrand accumet gel-filled pencil-thin pH combination electrode to monitor the pH during the reaction. While the reduction of ClO_3^- and ClO_2^- does not consume H^+, the reduction of NO_3^- consumes H^+ and may elevate the pH.[45] To maintain the solution pH at 7−8, H_2SO_4 (0.1 M) was added via the sampling needle when the pH reading went higher than 8.0.

Sample Analysis and Kinetic Evaluation. The concentrations of ClO_3^- and ClO_2^- were determined by ion chromatography (Dionex ICS-5000) equipped with a conductivity detector and an IonPac AS19 column. The column temperature was set at 30 °C, with 20 mM KOH eluent at 1 mL min^{-1}. The concentrations of Ru and Pd in aqueous samples were analyzed by ICP-OES (detection limit 10 $\mu g\ L^{-1}$).

https://doi.org/10.1021/acs.est.3c00415
Environ. Sci. Technol. 2023, 57, 3962−3970

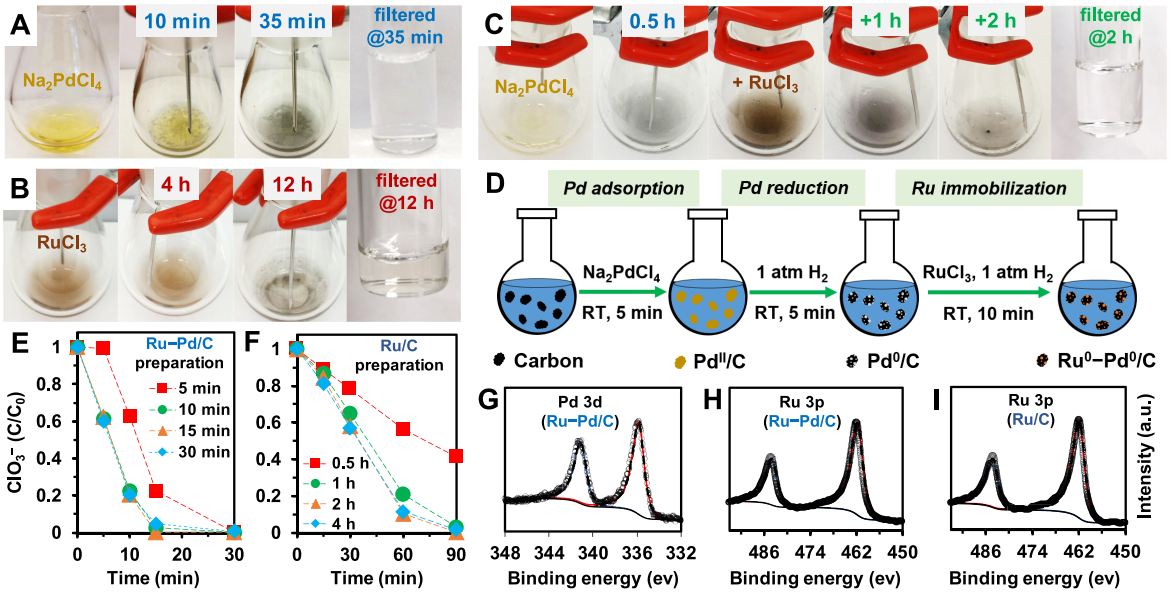

Figure 1. The reduction of (A) aqueous Pd^{II} (360 mg L^{-1} of Pd from Na_2PdCl_4), (B) aqueous Ru^{III} (40 mg L^{-1} of Ru from $RuCl_3$), and (C) first Pd^{II} (40 mg L^{-1}) then Ru^{III} (40 mg L^{-1}) by 1 atm H_2 (blown from the needle tip 5 mm above the liquid) at 20 °C. (D) The all-in situ procedure for Ru−Pd/C preparation. Profiles of ClO_3^- reduction by (E) Ru−Pd/C and (F) Ru/C after different durations of Ru^{III} reduction before adding ClO_3^-. Reaction conditions: 1 mM ClO_3^-, 0.1 g L^{-1} of 1 wt % Ru−1 wt % Pd/C or 1 wt % Ru/C, pH 7, 1 atm H_2, 20 °C. XPS spectra (empty dots) and fits (solid lines) of Pd 3d and Ru 3p of (G, H) Ru−Pd/C and (I) Ru/C.

When all ClO_3^- was reduced, the turnover number (TON) was calculated as

$$\mathrm{TON} = [\mathrm{ClO_3^-}]_0 \times M_w/(L_{cat} \times C_{metal} \times D_{metal})$$

where $[ClO_3^-]_0$ is the initial concentration of chlorate (mol L^{-1}), M_w is the atomic mass of Ru or Pd (g mol^{-1}), L_{cat} is the loading of catalyst powder (g L^{-1}), C_{metal} is the metal content, and D_{metal} is the metal dispersion.

The initial turnover frequency (TOF_0, in min^{-1}) was calculated as

$$\mathrm{TOF_0} = ([\mathrm{ClO_3^-}]_0 - [\mathrm{ClO_3^-}]_t) \times \mathrm{M_w} /(L_{cat.} \times C_{metal} \times D_{metal} \times t)$$

where $[ClO_3^-]_t$ is the concentration at the first sampling point of reaction time t (min).

RESULTS AND DISCUSSION

Catalyst Development. Both aqueous Ru^{III} (from $RuCl_3 \cdot xH_2O$) and Pd^{II} (from Na_2PdCl_4) can be reduced into Ru^0 and Pd^0 precipitates, respectively, by direct exposure to 1 atm H_2 in the headspace at 20 °C, but the reduction of Ru^{III} is much slower than that of Pd^{II}. While the yellow Pd^{II} solution was fully converted into Pd black (i.e., large Pd^0 solids) and colorless liquid within 35 min (Figure 1A),[28] the same procedure cannot complete the reduction of Ru^{III} by 12 h (Figure 1B). However, Ru^{III} added to the Pd black suspension underwent fast color fading and particle formation within 2.5 h (Figure 1C). Hence, Pd^0 accelerated the H_2 reduction of Ru^{III} into Ru^0. The adsorption behaviors of aqueous Ru^{III} and Pd^{II} on porous carbon support (1300 m^2 g^{-1}) were also different. While >98% of Pd^{II} was immobilized on carbon within 5 min,[28] only 84% of Ru^{III} was immobilized in the same time frame.

Inspired by the above phenomena, we prepared the bimetallic catalyst by adding Ru^{III} into the all-in situ prepared Pd^0/C (Figure 1D). In the nanoscale carbon pores, the highly dispersed Pd^0 particles were expected to provide a faster reduction of Ru^{III} than the bulky Pd black aggregates. The adsorption and reduction of Ru^{III} (onto Pd^0/C by 1 atm H_2 at 20 °C) for only 10 min yielded the full activity of ClO_3^- reduction (Figure 1E). The dissolved Pd and Ru in the aqueous phase were below 1 μg L^{-1}, showing that >99.9% of the two PGMs were immobilized. XPS measured the BE of Pd $3d_{5/2}$ at 335.8 eV and Ru $3p_{3/2}$ at 461.8 eV (Figure 1G,H), confirming the reduction of both metals to the metallic state. Therefore, only 20 min is needed to prepare Ru^0−Pd^0/C all-in situ from aqueous Ru^{III}, Pd^{II}, carbon support, and 1 atm H_2 at 20 °C.

We also directly immobilized Ru^{III} on the same carbon support without Pd^0. The adsorption of >95% Ru^{III} required 1 h (Figure S1A). Upon H_2 exposure for another 1 h, the fraction of dissolved Ru was further lowered to 0.2% (Figure S1B). XPS characterization confirmed the yield of Ru^0/C (Figure 1I, Ru $3p_{3/2}$ BE at 461.8 eV, the same as in Ru^0−Pd^0/C). More than 1 h of H_2 exposure was required to maximize the ClO_3^- reduction activity (Figure 1F). The three catalysts had consistent metal contents: 0.64 wt % of Pd in Pd^0/C, 0.68 wt % of Pd + 0.98 wt % of Ru in Ru^0−Pd^0/C, and 0.94 wt % of Ru in Ru^0/C. These values show the reliability of the all-in situ preparation method, which provides a fair basis for activity comparison. We further validated the all-in situ adsorption-reduction method for Ru/C by comparing it with the conventional incipient wetness + heated H_2 reduction method and a commercial catalyst (Figure S2).

Chlorate Reduction Performance. Based on the chemisorption data (Table 1) and ClO_3^- reduction time profile (Figure 2A), we calculated the initial turnover frequency (TOF_0, the average number of ClO_3^- anions reduced by individual surface metal atoms upon the first sampling time). At pH 7, Pd/C barely catalyzed ClO_3^- reduction (TOF_0 = 0.4 min^{-1} on Pd^0) while Ru/C was much more active (TOF_0 = 9.0 min^{-1} on Ru^0). Surprisingly, Ru−Pd/C was substantially more active than Ru/C. A conservative estimation of TOF_0 (see later sections for the

https://doi.org/10.1021/acs.est.3c00415
Environ. Sci. Technol. 2023, 57, 3962−3970

Table 1. Metal Dispersion from CO Chemisorption[a]

entry	catalyst	metal dispersion
1	Pd/C	20.9%
2	Ru/C	15.0%
3	Ru/C[b]	37.1%
4	Ru−Pd/C	36.5−42.5%[c]
5	Pd−Ru/C	25.0−29.2%[c]

[a]Unless specified, the catalysts were prepared by the all-in situ method with a nominal 1 wt % content for each metal. The stoichiometries for Ru:CO and Pd:CO are 12:7[41] and 2:1,[42] respectively. [b]Prepared by the conventional method involving incipient wetness impregnation and reduction with heated H_2 (see Materials and Methods section for details). [c]The lower and higher limits were calculated assuming all-Ru and all-Pd scenarios in the bimetallic system.

Table 2. Rate Constants of ClO_3^- Reduction by Ru−Pd/C Catalysts with Variable Formulations

entry	Pd (wt %)	Ru (wt %)	apparent rate ($mM\ min^{-1}$)[a]	metal-normalized rate ($mmol\ g_{metal}^{-1}\ min^{-1}$)[b]
1	5	5	0.116	11.6
2	3	3	0.114	19.1
3	1	1	0.091	45.3
4	1	0.1	0.010	9.2
5	1	0	0.001	0.8
6	0.1	1	0.024	21.5
7	0	1	0.014	14.3
8	0.5	0.5	0.040	40.1
9	0.1	0.1	0.009	44.0
10	1	1.5	0.096	38.3
11	1	0.5	0.052	34.9

[a]Reaction conditions: 0.1 g L^{-1} of Ru−Pd/C, 1 mM ClO_3^-, pH 7, 1 atm H_2, 20 °C. [b]Normalized to the total mass of Ru and Pd.

estimation of Ru dispersion) is 13.9 min^{-1} on Ru^0. A good mass balance of Cl was established between ClO_3^- and Cl^- (Figure 2B), indicating no accumulation of other chlorine species.

Because the all-in situ method allows rapid preparation of various catalyst formulations, we extensively screened Ru and Pd contents from 0.1 to 5 wt % and identified critical roles of both metals. First, the addition of Ru as low as 0.1 wt % can significantly enhance the activity of the monometallic Pd/C (Table 2, entry 4 versus 5) and vice versa (entry 6 versus 7), suggesting the synergy between Ru and Pd. The highest activity was shown when the two metals were both loaded at 1 wt %. An unexpected advantage of Ru−Pd/C over Ru/C was observed from the treatment of concentrated ClO_3^-. The use of 0.1 g/L of Ru−Pd/C achieved 99.9% reduction of 100 mM ClO_3^- (Figure 2C) with a TON (the total number of ClO_3^- anions reduced by each surface Ru atom) of 11,970. In contrast, Ru/C was substantially inhibited by the concentrated ClO_3^- (Figure 2C versus A). Second, increasing the metal contents above 1 wt % did not proportionally accelerate ClO_3^- reduction (Table 2, entries 1−3). Instead, the rate constant normalized by the total mass of Ru and Pd became lower, probably due to the decreased metal dispersion.[28] Third, decreasing the metal content below 1 wt % did not further increase the normalized rate (Table 2, entries 3, 8, and 9). In other words, in order to support the same amount of metal to achieve the same reaction rate, more carbon material needs to be used. Further fine-tuning of Ru content at 1.5 and 0.5 wt % in 1 wt % Pd/C did not yield better performance (Table 2, entries 10 and 11 versus 3). Thus, we kept using the 1 wt % formulation for both Ru and Pd.

Ru−Pd/C outperforms all reported PGM-based catalysts for ClO_3^- reduction in a wide pH range from 3 to 8. At pH 7, the metal-normalized first-order rate constant is more than two orders of magnitude higher than those of Rh/C[35] and Mo−Pd/C[34] (Figure 2D), both of which show the highest activity at pH 3. However, the activity of Ru−Pd/C also increased at pH 3, still being five to seven times more active than Rh/C and Mo−Pd/C under acidic conditions. The kinetics data fitting is discussed in detail in Text S1. Both internal and external mass transfer limitations are negligible (Text S2). A comprehensive comparison of all PGM catalysts is provided in Table S1. Although Rh/C is much more active than Pd/C for ClO_3^- reduction at pH 7 (Table S1, entry 4 versus 3), the Ru−Rh/C catalyst prepared by the same all-in situ method showed almost identical activity as Ru−Pd/C (Figure S3), corroborating the dominant role of Ru in the reaction with ClO_3^-. Thus, the use of Ru avoids the use of Rh and saves a substantial amount of Pd. Rh is 28 times more expensive than Ru,[46] while Pd is three times more expensive but three to four orders of magnitude less active than Ru. However, in comparison to the monometallic Ru/C, the significantly enhanced activity, robustness with concentrated ClO_3^-, and different pH dependence of Ru−Pd/C also suggest critical roles of Pd in the catalyst structure and reaction scheme.

Mechanistic Elucidation. High-angle annular dark-field scanning transmission electron microscopy (HAADF-STEM) characterization of Ru−Pd/C observed fine metal particles with an average size of 2.3 nm on the carbon support (Figure 3A,B,G,H). The size is apparently larger than Pd particles of Pd/

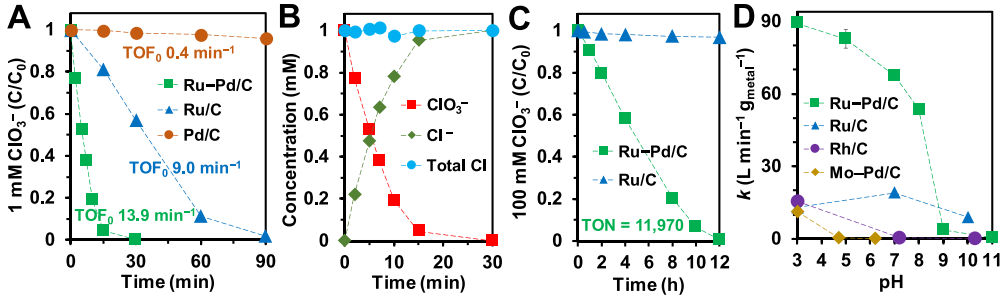

Figure 2. (A) Profiles and TOF_0 for 1 mM ClO_3^- reduction by three catalysts prepared by the all-in situ method. (B) Chlorine balance during ClO_3^- reduction. (C) Reduction of 100 mM ClO_3^- by Ru−Pd/C and Ru/C. (D) pH dependence of Ru−Pd/C, Ru/C, and previously reported 5 wt % Rh/C[35] and 5 wt % Mo−5 wt % Pd/C.[34] First-order rate constants were normalized by the loading of PGM. Reaction conditions: 0.1 g L^{-1} catalyst (1 wt % Ru and/or Pd), pH 7, 1 atm H_2, 20 °C.

https://doi.org/10.1021/acs.est.3c00415
Environ. Sci. Technol. 2023, 57, 3962−3970

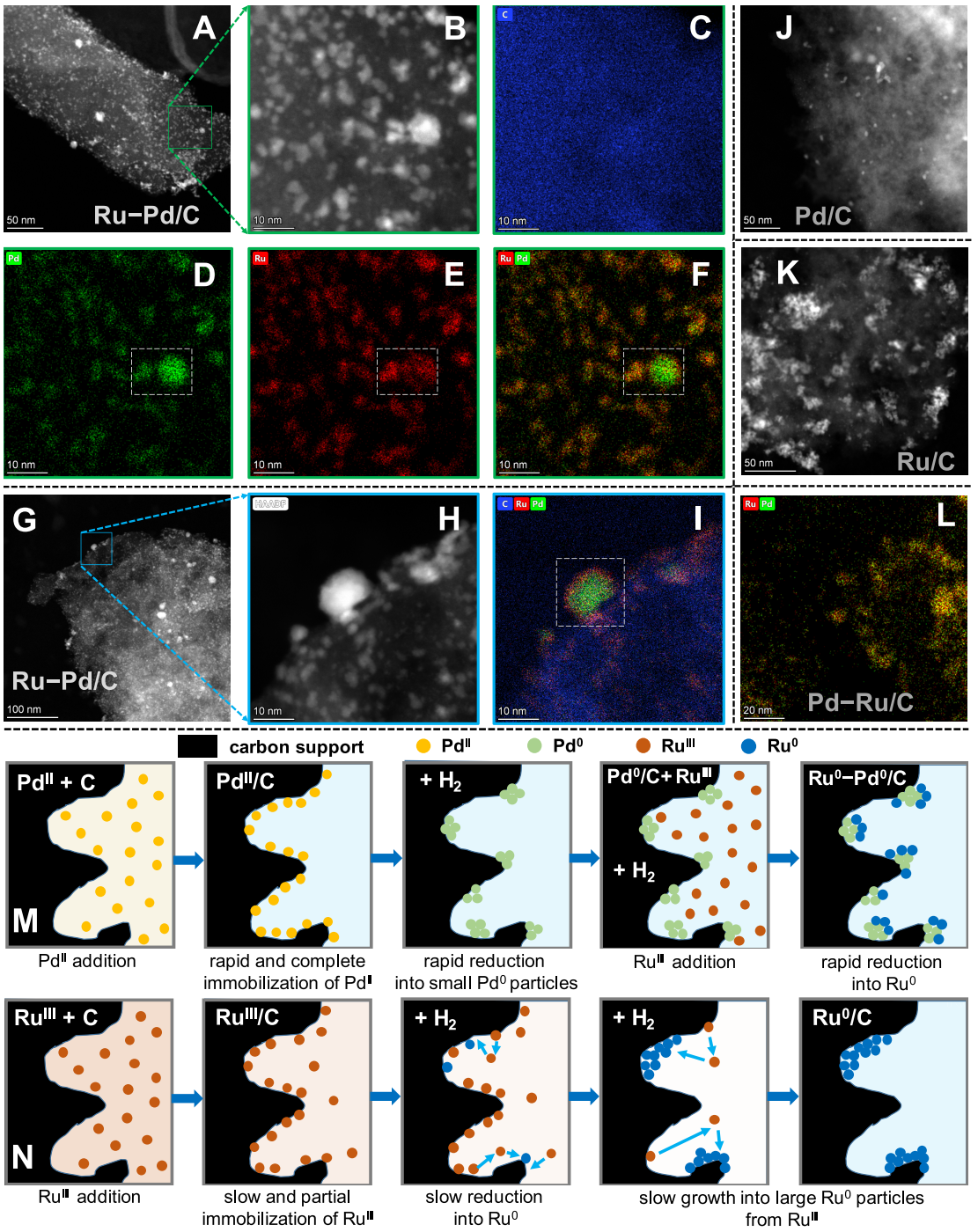

Figure 3. HAADF-STEM imaging of (A, B, G, and H) 1 wt % Ru−1 wt % Pd/C, (J) 1 wt % Pd/C, and (K) 1 wt % Ru/C prepared by the all-in situ method. (C, D, E, F, and I) EDS elemental mapping. (L) EDS mapping of 1 wt % Pd−1 wt % Ru/C. The dotted areas in D, E, F, and I highlight the Ru coverage outside Pd. Conceptual illustration of Ru and Pd particles formation in (M) Ru−Pd/C and (N) Ru/C.

C (<2 nm on average)[28] before accommodating Ru (Figure 3J versus A). EDS elemental mapping (Figure 3C−F) confirmed the bright spots as overlapped Pd and Ru. The relatively large particles clearly show the mixing pattern as a layer of Ru on the outside of Pd particles (Figure 3F,I). Hence, Ru^{III} was rapidly reduced as Ru^0 on Pd^0 particles by the on-surface active H (Figure 3M).[47] Besides, one cannot exclude the scenario that a minor fraction of Ru was reductively immobilized in the vicinity of Pd^0 particles by spilled-over H on the carbon support.[48]

In stark contrast, the direct reduction of Ru^{III} on carbon resulted in large aggregates (Figure 3K). In comparison to Pd^{II}, the poorer adsorption of Ru^{III} and much slower reduction (by H_2 at 20 °C) can be responsible for such morphology (Figure 3N). Relatively few Ru^0 seeds can form at the beginning, and the remaining Ru^{III} can migrate to the surface or vicinity of existing Ru^0 particles, slowly react with the active H, and gradually yield the bulky Ru^0 solid. The integration of Pd^0 with Ru^0/C was also achieved. Elemental mapping of Pd−Ru/C found the overlapping of Pd and Ru in much larger aggregates than in Ru−Pd/C (Figure 3L versus F, note the scale). Not surprisingly, the ClO_3^- reduction activity of Pd−Ru/C was only 43% of that of Ru−Pd/C (Figure S4).

https://doi.org/10.1021/acs.est.3c00415
Environ. Sci. Technol. 2023, 57, 3962−3970

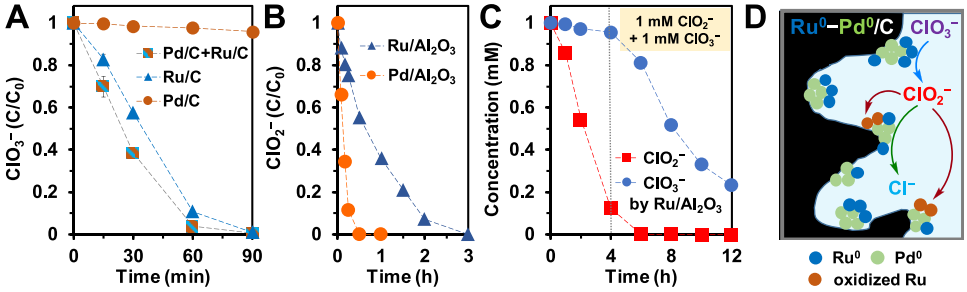

Figure 4. Profiles of (A) ClO_3^- reduction by individual Ru/C, Pd/C, and 1:1 mixed Ru/C + Pd/C at pH 7. (B) ClO_2^- reduction at pH 7.9 by Ru/Al_2O_3 and Pd/Al_2O_3. (C) ClO_2^- and ClO_3^- reduction in the mixture by Ru/Al_2O_3 at pH 7.9. Default reaction conditions: 0.1 g L^{-1} of individual catalyst containing 1 wt % of metal, 1 mM ClO_3^- or ClO_2^-, 1 atm H_2, 20 °C. (D) Illustrated reaction mechanisms on the Ru−Pd/C catalyst surface.

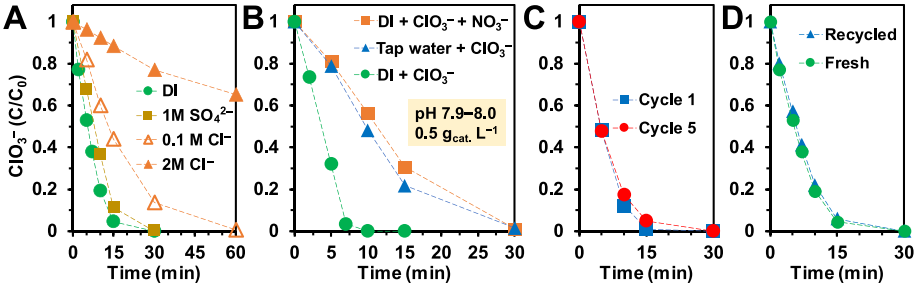

Figure 5. Profiles of ClO_3^- reduction (A) in the presence of Cl^- and SO_4^{2-}, (B) in tap water (pH 7.9) and DI water with and without 0.4 mM NO_3^- (pH 8.0) at 0.5 g L^{-1} catalyst loading, (C) in the first and fifth ClO_3^- spikes (1 mM) in the same batch reactor, and (D) in the as-prepared catalyst suspension and by the centrifuge-collected and redispersed catalyst. Default reaction conditions: 0.1 g L^{-1} of 1 wt % Ru−1 wt % Pd/C, 1 mM ClO_3^-, pH 7, 1 atm of H_2, 20 °C.

The CO chemisorption data indicate substantially enhanced metal dispersion in the bimetallic catalysts (Table 1). The dispersion is measured as the percentage of surface Ru and Pd atoms exposed to CO, which roughly simulates the accessibility for the aqueous oxyanion substrates. While the Pd dispersion in Pd/C was 20.9%, the total metal dispersion in Ru−Pd/C ranged from 36.5% (all Ru) to 42.5% (all Pd), based on the stoichiometry for Ru:CO (12:7) and Pd:CO (2:1). Without a high-temperature process, the later added Ru is less likely to change the morphology of Pd. Thus, the enhanced dispersion in Ru−Pd/C should be attributed to high dispersion of Ru ranging from 55% (if Pd and Ru did not overlap at all, see Text S3 for calculation) to 85% (if Pd was completely covered by Ru). This value is higher than Ru/C prepared by the conventional method (37.1%), which accelerated metal reduction by heated H_2. Similarly, the total metal dispersion in Pd−Ru/C (25.0−29.2%) is also higher than Ru/C (15.0%). In comparison to Pd/C (20.9% dispersion), Ru enhanced the Pd dispersion in Pd−Ru/C to the calculated 35−58%.

The >55% dispersion of Ru in Ru−Pd/C can contribute to the higher ClO_3^- reduction activity than Pd−Ru/C (dispersion of Ru <15% due to Pd coverage). However, the higher activity of Pd−Ru/C (k = 2.3 mM h^{-1}) than Ru/C (k = 0.9 mM h^{-1}) suggests other critical roles of Pd. Despite the negligible activity of Pd/C at pH 7, a 1:1 mixture of the two monometallic Pd/C and Ru/C catalysts exhibited a higher activity than using Ru/C only (Figure 4A). Thus, we further probed the individual activity of Ru and Pd with ClO_2^-, the most probable first intermediate from ClO_3^- reduction. Since ClO_2^- can react with carbon,[49,50] we prepared Pd/Al_2O_3 and Ru/Al_2O_3 with the same all-in situ method.[28] Pd/Al_2O_3 showed 5.4-fold higher activity of ClO_2^- reduction than Ru/Al_2O_3 (Figure 4B). More interestingly, when 1:1 of ClO_3^- and ClO_2^- was added together to Ru/Al_2O_3, the reduction of ClO_3^- was largely inhibited until >90% of ClO_2^- was reduced first (Figure 4C). Therefore, the very low apparent activity in treating 100 mM ClO_3^- (Figure 2C) and the inhibition of a commercial Ru/C in our previous study[35] are likely attributed to the accumulation of ClO_2^- shortly after the reaction. Reactions of Ru species with ClO_2^- (and the potential daughter product ClO^-) are complex. For example, bulk Ru^0 can be oxidized by concentrated ClO^- toward dissolution;[51] oxidized Ru species such as Ru^{II} and H^+ can trigger complex decomposition of ClO_2^- into ClO_2, HOCl, ClO_3^-, and Cl^-.[44,52] Details of these reactions remain largely unexplored and warrant further investigation. Nevertheless, the findings above clearly suggest the synergy between Ru^0 and Pd^0; Ru reduces ClO_3^- for a fast overall reaction while Pd rapidly scavenges ClO_x^- and generates active H to minimize the oxidative deactivation of Ru (Figure 4D). The oxidized Ru can still be reduced back to Ru^0 by Pd-activated H_2 (Figures 1C and 3M).

Catalyst Robustness. We assessed the performance of Ru−Pd/C for ClO_3^- reduction in typical application scenarios, such as (i) chloralkali NaCl brines containing the undesirable ClO_3^- byproduct from the anode,[32] (ii) waste stream from reverse osmosis or ion exchange that enriched ClO_3^- from source water, and (iii) drinking water containing ClO_3^- from source water or disinfection operations.[2] Because modern water treatment usually involves sequential processes and does not expose advanced systems to raw water or known poisoning/destructive species,[30,53] we did not intentionally challenge the catalyst with sulfide (a potent PGM catalyst poison but readily oxidizable)[54] or humic acid (a common fouling species but readily adsorbable).[29] Instead, anions such as Cl^- and SO_4^{2-} are ubiquitous co-existing species. The presence of 1.0 M SO_4^{2-}, 0.1 M Cl^-, and 2.0 M Cl^- decreased the rate of 1 mM ClO_3^- reduction for 30, 58, and 94%, respectively (Figure 5A). Even

https://doi.org/10.1021/acs.est.3c00415
Environ. Sci. Technol. 2023, 57, 3962−3970

under the inhibition by 2.0 M Cl^-, the reduction of 1 mM ClO_3^- was completed within 8 h (Figure S5). Thus, a higher loading of catalyst can be used to proportionally boost the apparent reaction rate.[30,55]

We also tested Ru−Pd/C in a tap water sample from Southern California, where the groundwater occasionally contained ClO_3^- slightly higher than the minimum reporting level (0.02 mg L^{-1}, or 0.24 μM). The tap water had an initial pH of 7.9 and also contained 0.4 mM NO_3^-. The use of 0.5 g L^{-1} Ru−Pd/C reduced the spiked 1 mM ClO_3^- for 99, 99.95, and >99.99% (i.e., lower than the detection limit of 0.1 μM) within 30, 45, and 60 min, respectively (Figure 5B). However, the reaction rate was slower than in the deionized (DI) water. The addition of 0.4 mM NO_3^- in DI water resulted in a very similar level of inhibition as in the tap water. Therefore, other constituents in the tap water were not significant inhibitors of Ru−Pd/C. This catalyst showed a relatively low activity for NO_3^- reduction at pH 8, and NO_3^- reduction barely proceeded before the majority of ClO_3^- was reduced (Figure S6).

Preliminary reuse tests show that Ru−Pd/C did not lose activity after five spikes of 1 mM ClO_3^- (Figure 5C) because the inhibition by Cl^- in the mM concentration range is negligible. Centrifugation and handling in the air did not deactivate the recycled catalyst (Figure 5D). The PGM leaching into the water was below the detection limit (10 μg L^{-1}; i.e., <1% of the immobilized 1 wt % Ru or Pd) from these operations.

Implications to Reductive Catalysis Technology for Water Treatment. This study demonstrates the use of rational chemistry design and simple engineering approaches to develop catalysts tailored for water treatment applications. It has significantly advanced the technology in the following aspects. (i) *Facile catalyst preparation*: a highly active Ru−Pd/C catalyst is conveniently prepared by sequential all-in situ adsorption−reduction of Pd^{II} and Ru^{III} precursors on the carbon support. The preparation only takes 20 min using 1 atm H_2 at 20 °C without heating procedures (Figure 1D,E). (ii) *Unprecedented catalyst performance*: the Pd^0 nanoparticles accelerate the reduction of Ru^{III} into highly dispersed (>55%) Ru^0. The resulting Ru−Pd/C catalyst shows a substantially higher activity of ClO_3^- reduction into Cl^- than any reported catalyst at both neutral and acidic pH (Figure 2D and Table S1). (iii) *High robustness under various conditions*: the catalyst allows complete reduction of ClO_3^-, from 100 mM to 0.1 μM, in the presence of concentrated SO_4^{2-} and Cl^-, as well as in the tap water matrix (Figure 5). (iv) *Confirmed bimetallic synergy*: while Ru shows high reactivity with ClO_3^-, Pd is more reactive with ClO_2^-, which is an inhibitor of Ru (Figure 4). The synergy between Ru and Pd makes Ru−Pd/C superior to monometallic Ru/C and Pd/C, especially in reducing concentrated ClO_3^- (Figure 2C). Hence, this work showcases a novel and robust catalyst to solve the recently recognized ClO_3^- challenge at the water−energy−food nexus.

In particular, Ru−Pd/C showing a very high activity at pH 7 makes it feasible to treat ClO_3^- under various water conditions. Further evaluation of catalyst performance in specific application scenarios is warranted. The challenge of ClO_3^- in various water treatment systems is emerging (i.e., frequently observed but not solved). Particular needs and further demonstration for integrating the catalytic system in the existing water treatment systems, such as chlorination and electrochemical treatment, are to be identified by end users. The current challenges and knowledge gaps in treating per- and polyfluoroalkyl substances (PFAS) have proved the importance of preparing innovative technologies for various recalcitrant chemicals before regulatory decisions.

■ ASSOCIATED CONTENT

Supporting Information

The Supporting Information is available free of charge at https://pubs.acs.org/doi/10.1021/acs.est.3c00415.

Kinetic data of catalysts reported in literature, prepared by other methods, or tested under specific conditions; discussion on reaction kinetics fitting and mass transfer limitation; and estimation of metal dispersion in the bimetallic catalyst (PDF)

■ AUTHOR INFORMATION

Corresponding Author

Jinyong Liu − *Department of Chemical & Environmental Engineering, University of California, Riverside, California 92521, United States;* orcid.org/0000-0003-1473-5377; Email: jinyong.liu101@gmail.com

Authors

Jinyu Gao − *Department of Chemical & Environmental Engineering, University of California, Riverside, California 92521, United States;* orcid.org/0000-0002-1751-3430

Shaohua Xie − *Department of Civil, Environmental, and Construction Engineering, Catalysis Cluster for Renewable Energy and Chemical Transformations (REACT), NanoScience Technology Center (NSTC), University of Central Florida, Orlando, Florida 32816, United States;* orcid.org/0000-0003-1550-7421

Fudong Liu − *Department of Civil, Environmental, and Construction Engineering, Catalysis Cluster for Renewable Energy and Chemical Transformations (REACT), NanoScience Technology Center (NSTC), University of Central Florida, Orlando, Florida 32816, United States;* orcid.org/0000-0001-8771-5938

Complete contact information is available at: https://pubs.acs.org/10.1021/acs.est.3c00415

Notes

The authors declare no competing financial interest.

■ ACKNOWLEDGMENTS

Financial support was provided by the National Science Foundation (CBET-1932942 for J.G. and J.L.). F.L. acknowledges the Startup Fund from the University of Central Florida (UCF). S.X. thanks the support from the Preeminent Postdoctoral Program (P3) at UCF. Dr. Krassimir Bozhilov performed the STEM characterization at the Central Facility for Advanced Microscopy and Microanalysis (CFAMM) at UC Riverside. Dr. Ich Tran assisted in the XPS characterization performed at the UC Irvine Materials Research Institute (IMRI) using instrumentation funded in part by the National Science Foundation Major Research Instrumentation Program (CHE-1338173).

■ REFERENCES

(1) *Expert Market Research. Sodium chlorate market size, share, analysis, trends and forecast 2021−2026*; 2020. https://www.researchandmarkets.com/reports/5323457 (accessed July 5, 2022).

(2) Gorzalski, A. S.; Spiesman, A. L. Insights on Chlorate Occurrence, Intra-system Variability, and Source Water Concentrations. *J. Am. Water Works Assoc.* **2015**, *107*, E613−E626.
(3) Karlsson, R. K.; Cornell, A. Selectivity between oxygen and chlorine evolution in the chlor-alkali and chlorate processes. *Chem. Rev.* **2016**, *116*, 2982−3028.
(4) Lakshmanan, S.; Murugesan, T. The chlor-alkali process: work in progress. *Clean Technol. Environ. Policy* **2014**, *16*, 225−234.
(5) Park, H.; Vecitis, C. D.; Hoffmann, M. R. Electrochemical Water Splitting Coupled with Organic Compound Oxidation: The Role of Active Chlorine Species. *J. Phys. Chem. C* **2009**, *113*, 7935−7945.
(6) Kumar, A.; Phillips, K. R.; Thiel, G. P.; Schröder, U.; Lienhard, J. H. Direct electrosynthesis of sodium hydroxide and hydrochloric acid from brine streams. *Nat. Catal.* **2019**, *2*, 106.
(7) Cho, K.; Qu, Y.; Kwon, D.; Zhang, H.; Cid, C. M. A.; Aryanfar, A.; Hoffmann, M. R. Effects of anodic potential and chloride ion on overall reactivity in electrochemical reactors designed for solar-powered wastewater treatment. *Environ. Sci. Technol.* **2014**, *48*, 2377−2384.
(8) Ibl, N.; Landolt, D. On the mechanism of anodic chlorate formation in dilute NaCl solutions. *J. Electrochem. Soc.* **1968**, *115*, 713−720.
(9) Landolt, D.; Ibl, N. On the mechanism of anodic chlorate formation in concentrated NaCl solutions. *Electrochim. Acta* **1970**, *15*, 1165−1183.
(10) Mastrocicco, M.; Di Giuseppe, D.; Vincenzi, F.; Colombani, N.; Castaldelli, G. Chlorate origin and fate in shallow groundwater below agricultural landscapes. *Environ. Pollut.* **2017**, *231*, 1453−1462.
(11) Rosemarin, A.; Lehtinen, K.-J.; Notini, M.; Mattson, J. Effects of pulp mill chlorate on Baltic Sea algae. *Environ. Pollut.* **1994**, *85*, 3−13.
(12) Stauber, J. L. Toxicity of chlorate to marine microalgae. *Aquat. Toxicol.* **1998**, *41*, 213−227.
(13) McCarthy, W. P.; O'Callaghan, T. F.; Danahar, M.; Gleeson, D.; O'Connor, C.; Fenelon, M. A.; Tobin, J. T. Chlorate and other oxychlorine contaminants within the dairy supply chain. *Compr. Rev. Food Sci. Food Saf.* **2018**, *17*, 1561−1575.
(14) Kettlitz, B.; Kemendi, G.; Thorgrimsson, N.; Cattoor, N.; Verzegnassi, L.; Le Bail-Collet, Y.; Maphosa, F.; Perrichet, A.; Christall, B.; Stadler, R. H. Why chlorate occurs in potable water and processed foods: a critical assessment and challenges faced by the food industry. *Food Addit. Contam., Part A* **2016**, *33*, 968−982.
(15) Li, M.; Xiao, M.; Xiao, Q.; Chen, Y.; Guo, Y.; Sun, J.; Li, R.; Li, C.; Zhu, Z.; Qiu, H.; Liu, X.; Lu, S. Perchlorate and chlorate in breast milk, infant formulas, baby supplementary food and the implications for infant exposure. *Environ. Int.* **2022**, *158*, 106939.
(16) Liu, Q.; Mao, W.; Jiang, D.; Yang, X.; Yang, D. The contamination and estimation of dietary intake for perchlorate and chlorate in infant formulas in China. *Food Addit. Contam., Part A* **2021**, *38*, 2045−2054.
(17) EFSA CONTAM Panel. Scientific opinion on risks for public health related to the presence of chlorate in food. *EFSA J* **2015**, *13*, 4135.
(18) Smith, D. J.; Taylor, J. B. Chlorate Analyses in Matrices of Animal Origin. *J. Agric. Food Chem.* **2011**, *59*, 1598−1606.
(19) Panseri, S.; Nobile, M.; Arioli, F.; Biolatti, C.; Pavlovic, R.; Chiesa, L. M. Occurrence of perchlorate, chlorate and polar herbicides in different baby food commodities. *Food Chem.* **2020**, *330*, 127205.
(20) Alfredo, K.; Stanford, B.; Roberson, J. A.; Eaton, A. Chlorate Challenges for Water Systems. *J. Am. Water Works Assoc.* **2015**, *107*, 187.
(21) WHO *Chlorite and Chlorate in Drinking-Water: Background Document for Development of WHO Guidelines for Drinking-Water Quality; WHO/SDE/WSH/05.08/86*; World Health Organization, 2005.
(22) European Union. Directive (EU) 2020/2184 of the European Parliament and of the Council of 16 December 2020 on the quality of water intended for human consumption (recast) (Text with EEA relevance). *Off. J. Eur. Union* **2020**, 1−62.
(23) SAC *National standard of the People's Republic of China: standards for drinking water quality; GB 5749−2022*; Standardization Administration of China, 2022.
(24) EPA *Six-Year Review 3 Technical Support Document for Chlorate; EPA-810-R-16-013*; U.S. Environmental Protection Agency, Office of Water, 2016.
(25) U.S. Environmental Protection Agency. Revisions to the unregulated contaminant monitoring regulation (UCMR 3) for public water systems. *Fed. Regist.* **2012**, *77*, 26072−26101.
(26) Saguru, C.; Ndlovu, S.; Moropeng, D. A review of recent studies into hydrometallurgical methods for recovering PGMs from used catalytic converters. *Hydrometallurgy* **2018**, *182*, 44−56.
(27) De Corte, S.; Hennebel, T.; De Gusseme, B.; Verstraete, W.; Boon, N. Bio-palladium: from metal recovery to catalytic applications. *Microb. Biotechnol.* **2012**, *5*, 5−17.
(28) Gao, J.; Ren, C.; Huo, X.; Ji, R.; Wen, X.; Guo, J.; Liu, J. Supported Palladium Catalysts: A Facile Preparation Method and Implications to Reductive Catalysis Technology for Water Treatment. *ACS ES&T Eng.* **2021**, *1*, 562−570.
(29) Chaplin, B. P.; Reinhard, M.; Schneider, W. F.; Schüth, C.; Shapley, J. R.; Strathmann, T. J.; Werth, C. J. Critical review of Pd-based catalytic treatment of priority contaminants in water. *Environ. Sci. Technol.* **2012**, *46*, 3655−3670.
(30) Ren, C.; Bi, E. Y.; Gao, J.; Liu, J. Molybdenum-Catalyzed Perchlorate Reduction: Robustness, Challenges, and Solutions. *ACS ES&T Eng.* **2022**, *2*, 181−188.
(31) Van Santen, R.; Klesing, A.; Neuenfeldt, G.; Ottmann, A. Method for removing chlorate ions from solutions. U.S. Patent 6,270,682, 2001.
(32) Kuznetsova, L. I.; Kuznetsova, N. I.; Koscheev, S. V.; Zaikovskii, V. I.; Lisitsyn, A. S.; Kaprielova, K. M.; Kirillova, N. V.; Twardowski, Z. Carbon-supported iridium catalyst for reduction of chlorate ions with hydrogen in concentrated solutions of sodium chloride. *Appl. Catal., A: Gen.* **2012**, *427*, 8−15.
(33) Ye, T.; Banek, N. A.; Durkin, D. P.; Hu, M.; Wang, X.; Wagner, M. J.; Shuai, D. Pd nanoparticle catalysts supported on nitrogen-functionalized activated carbon for oxyanion hydrogenation and water purification. *ACS Appl. Nano Mater.* **2018**, *1*, 6580−6586.
(34) Ren, C.; Yang, P.; Gao, J.; Huo, X.; Min, X.; Bi, E. Y.; Liu, Y.; Wang, Y.; Zhu, M.; Liu, J. Catalytic Reduction of Aqueous Chlorate With MoOx Immobilized on Pd/C. *ACS Catal.* **2020**, *10*, 8201−8211.
(35) Chen, X.; Huo, X.; Liu, J.; Wang, Y.; Werth, C. J.; Strathmann, T. J. Exploring beyond palladium: Catalytic reduction of aqueous oxyanion pollutants with alternative platinum group metals and new mechanistic implications. *Chem. Eng. J.* **2017**, *313*, 745−752.
(36) Lin, B.; Heng, L.; Fang, B.; Yin, H.; Ni, J.; Wang, X.; Lin, J.; Jiang, L. Ammonia synthesis activity of alumina-supported ruthenium catalyst enhanced by alumina phase transformation. *ACS Catal.* **2019**, *9*, 1635−1644.
(37) Jang, H.; Kim, S.-H.; Lee, D.; Shim, S. E.; Baeck, S.-H.; Kim, B. S.; Chang, T. S. Hydrogenation of lactic acid to propylene glycol over a carbon-supported ruthenium catalyst. *J. Mol. Catal. A: Chem.* **2013**, *380*, 57−60.
(38) Hong, U. G.; Park, H. W.; Lee, J.; Hwang, S.; Song, I. K. Hydrogenation of succinic acid to γ-butyrolactone (GBL) over ruthenium catalyst supported on surfactant-templated mesoporous carbon. *J. Ind. Eng. Chem.* **2012**, *18*, 462−468.
(39) Karim, A. M.; Prasad, V.; Mpourmpakis, G.; Lonergan, W. W.; Frenkel, A. I.; Chen, J. G.; Vlachos, D. G. Correlating particle size and shape of supported Ru/γ-Al_2O_3 catalysts with NH3 decomposition activity. *J. Am. Chem. Soc.* **2009**, *131*, 12230−12239.
(40) Lin, B.; Wei, K.; Ni, J.; Lin, J. KOH activation of thermally modified carbon as a support of Ru catalysts for ammonia synthesis. *ChemCatChem* **2013**, *5*, 1941−1947.
(41) Chen, Q.; Liu, J.; Zhou, X.; Shang, J.; Zhang, Y.; Shao, X.; Wang, Y.; Li, J.; Chen, W.; Xu, G.; Wu, K. Unveiling structural evolution of CO adsorption on Ru (0001) with high-resolution STM. *J. Phys. Chem. C* **2015**, *119*, 8626−8633.
(42) Hooshmand, Z.; Le, D.; Rahman, T. S. CO adsorption on Pd (111) at 0.5 ML: A first principles study. *Surf. Sci.* **2017**, *655*, 7−11.

https://doi.org/10.1021/acs.est.3c00415
Environ. Sci. Technol. 2023, 57, 3962−3970

(43) Lebedeva, A.; Albuquerque, B. L.; Domingos, J. B.; Lamonier, J.-F. O.; Giraudon, J.-M.; Lecante, P.; Denicourt-Nowicki, A.; Roucoux, A. Ruthenium Trichloride Catalyst in Water: Ru Colloids versus Ru Dimer Characterization Investigations. *Inorg. Chem.* **2019**, *58*, 4141−4151.
(44) Deshwal, B. R.; Jo, H. D.; Lee, H. K. Reaction kinetics of decomposition of acidic sodium chlorite. *Can. J. Chem. Eng.* **2004**, *82*, 619−623.
(45) Liu, J.; Jong Kwon, C.; Sasnow, Z.; Werth, C. J.; Strathmann, T. J. Application of a Re-Pd bimetallic catalyst for treatment of perchlorate in waste ion-exchange regenerant brine. *Water Res.* **2013**, *47*, 91−101.
(46) Matthey, J. *Precious metals management*; https://platinum.matthey.com (accessed July 5, 2022).
(47) Conrad, H.; Ertl, G.; Latta, E. Adsorption of hydrogen on palladium single crystal surfaces. *Surf. Sci.* **1974**, *41*, 435−446.
(48) Prins, R. Hydrogen Spillover Facts and Fiction. *Chem. Rev.* **2012**, *112*, 2714−2738.
(49) Voudrias, E.; Dielmann, L., III; Snoeyink, V. L.; Larson, R. A.; McCreary, J.; Chen, A. Reactions of chlorite with activated carbon and with vanillic acid and indan adsorbed on activated carbon. *Water Res.* **1983**, *17*, 1107−1114.
(50) Gonce, N.; Voudrias, E. A. Removal of chlorite and chlorate ions from water using granular activated carbon. *Water Res.* **1994**, *28*, 1059−1069.
(51) Howe, J. L.; Mercer, F. N. Contributions to the study of ruthenium IX. Solubility of ruthenium in hypochlorite solutions and an attempt to utilize the reaction for the quantitative determination of the metal. *J. Am. Chem. Soc.* **1925**, *47*, 2926−2932.
(52) Hu, Z.; Du, H.; Man, W.-L.; Leung, C.-F.; Liang, H.; Lau, T.-C. Catalytic reactions of chlorite with a polypyridylruthenium (II) complex: disproportionation, chlorine dioxide formation and alcohol oxidation. *Chem. Commun.* **2012**, *48*, 1102−1104.
(53) Anis, S. F.; Hashaikeh, R.; Hilal, N. Reverse osmosis pretreatment technologies and future trends: A comprehensive review. *Desalination* **2019**, *452*, 159−195.
(54) Tomar, M.; Abdullah, T. H. Evaluation of chemicals to control the generation of malodorous hydrogen sulfide in waste water. *Water Res.* **1994**, *28*, 2545−2552.
(55) Ren, C.; Yang, P.; Sun, J.; Bi, E. Y.; Gao, J.; Palmer, J.; Zhu, M.; Wu, Y.; Liu, J. A Bioinspired Molybdenum Catalyst for Aqueous Perchlorate Reduction. *J. Am. Chem. Soc.* **2021**, *143*, 7891−7896.

https://doi.org/10.1021/acs.est.3c00415
Environ. Sci. Technol. 2023, 57, 3962−3970